First-Principles Vibrational Electron Energy Loss Spectroscopy of β-Guanine

G. Radtke,* D. Taverna, M. Lazzeri, and E. Balan
Institut de Minéralogie, de Physique des Matériaux, et de Cosmochimie (IMPMC) Sorbonne Universités—UPMC Univ Paris 06, UMR CNRS 7590, Muséum National d'Histoire Naturelle, IRD UMR 206, 4 Place Jussieu, F-75005 Paris, France
(Received 24 March 2017; published 13 July 2017)

A general approach to model vibrational electron energy loss spectra obtained using an electron beam positioned away from the specimen is presented. The energy-loss probability of the fast electron is evaluated using first-principles quantum mechanical calculations (density functional theory) of the dielectric response of the specimen. The validity of the method is assessed using recently measured anhydrous β-guanine, an important molecular solid used by animals to produce structural colors. The good agreement between theory and experiments lays the basis for a quantitative interpretation of this spectroscopy in complex systems.

DOI: 10.1103/PhysRevLett.119.027402

Until recently, the energy resolution of electron energy loss spectroscopy (EELS) as implemented in the transmission electron microscope (TEM) was too poor to reach the range of frequencies typically involved in vibrational excitations in most materials. Recent instrumental developments, however, leading not only to an improvement of the energy resolution down to less than 10 meV but also to a drastic reduction of the tail of the zero-loss peak, previously obscuring the infrared spectral region, now makes the detection of well-defined vibrational signatures possible for a wide range of materials with an unprecedented spatial resolution [1–3].

It is convenient to distinguish two regimes when considering the vibrational excitations induced by electrons which, borrowing the terminology employed in high-resolution EELS [4] (HREELS), are respectively named *impact* and *dipole* scattering regimes. Whereas the former becomes significant when large momentum transfers are selected and has been recently shown to allow for a mapping of vibrational modes with a spatial resolution of the order of the nanometer [5–7], the latter dominates at low-scattering angles, or, equivalently, small momentum transfers, and is largely delocalized in nature [8]. Of course, this distinction is artificial as one moves continuously from one regime to the other while increasing, or decreasing, the momentum transfer.

Dipole scattering is produced by long-range dipolar electric fields generated by molecular or lattice vibrations. As already stressed in Ref. [2], this effect is highly beneficial when investigating beam-sensitive specimens. Indeed, it provides an opportunity to carry out vibrational EELS using a beam positioned a few tens of nanometers away from the specimen (the so called "aloof" mode). When compared with an experiment performed with the same electron energy in a standard transmission geometry, this acquisition mode reduces the sample damage by a typical factor of 10^3 [9]. It can be easily anticipated that numerous applications of this technique in physical, earth, or life sciences will require the damage-free acquisition of vibrational spectra on radiation-sensitive materials and therefore rely on this specific geometry [1,2,10]. Moreover, this acquisition mode is inherently associated with spatially resolved EELS of nanostructures, a technique recently employed to map surface phonons in MgO nanocubes [3].

Crystals containing a large number of atoms per unit-cell, molecules and more generally, complex systems containing covalently bonded hydrogen display a large number of vibrational modes, hindering a straightforward interpretation of their spectra based on a simple comparison with known references or empirical models. A proper assessment of the origin of the different structures observed experimentally therefore relies on first-principles calculations.

In this Letter, we present a first-principles computational approach to model vibrational electron energy loss spectra acquired in aloof geometry. The approach uses density functional theory (DFT) and its effectiveness is demonstrated through the calculation and the analysis of the vibrational spectrum of biogenic anhydrous guanine extracted from Japanese koi fish scales [2].

This material, widespread in the animal kingdom and used for producing structural colors [11,12], crystallizes in a monoclinic structure ($P112_1/b$ space group), named β-guanine, and is built on the 7H-1H-amino-oxo tautomer [13]. The structure of the almost planar H-bonded molecular layers lying parallel to the crystal b-c plane is shown in Fig. 1. Note that the "staircase" like stacking of these layers along the a axis is not shown for clarity.

The simplest geometry which can be employed to approximately describe the experimental setup consists in an electron traveling along a rectilinear trajectory parallel to, and at a finite distance b from, the surface of a specimen occupying a half-space, as shown in Fig. 1(c). In a classical,

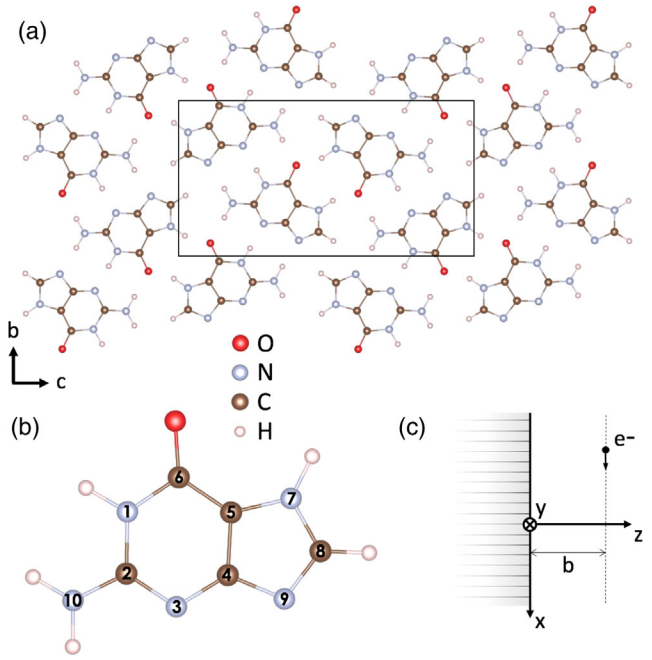

FIG. 1. Structure of β-guanine. (a) Global arrangement of the molecules in the crystal b-c plane; the monoclinic unit-cell containing four molecules is highlighted. (b) Structure of the molecule on which β-guanine is built, corresponding to the 7H-1H-amino-oxo tautomer. Atom numbering employed in this Letter is indicated. (c) Idealized geometry of the experiment: the specimen is described as a dielectric medium occupying a half-space ($z < 0$) while the probe electron travels in the vacuum along x at a constant distance b (impact parameter) from the interface.

quasistatic approach [14–16], the energy loss probability per unit angular frequency $dP(\omega,\mathsf{b})/d\omega$, associated with the energy $\hbar\omega$, is related to the work, W, done on the electron

$$W(\mathsf{b}) = \int_0^\infty \hbar\omega \frac{dP(\omega,\mathsf{b})}{d\omega} d\omega = -e\int_{-\infty}^{\infty} \mathbf{v}\cdot\mathbf{E}^{\mathrm{ind}}(\mathbf{r}_e)dt \tag{1}$$

where e is the elementary charge, $\mathbf{v}$ is the electron velocity, $\mathbf{E}^{\mathrm{ind}}(\mathbf{r}_e)$ is the electric field acting on the electron at position $\mathbf{r}_e$, and the last integration is performed on time t. We need to distinguish between the applied electric field, generated by the electron in the vacuum, $\mathbf{E}^{\mathrm{appl}}$, and that induced by the presence of the specimen which is polarized by the electron, $\mathbf{E}^{\mathrm{ind}}$. The Fourier components of the two associated potentials are related by $V^{\mathrm{ind}}(\omega,\mathbf{k}) = \alpha(\omega,\mathbf{k})V^{\mathrm{appl}}(\omega,\mathbf{k})$, where $\alpha(\omega,\mathbf{k})$ is the polarizability of the interface, calculated by solving Laplace's equation and imposing the continuity conditions at the interface between the vacuum half-space (where the electron travels) and the specimen half-space. In this region, Laplace's equation takes the form $\nabla[\overleftrightarrow{\epsilon}(\omega)\nabla V] = 0$, where $\overleftrightarrow{\epsilon}(\omega)$ is the local $[\overleftrightarrow{\epsilon}(\omega) \equiv \overleftrightarrow{\epsilon}(\mathbf{k}=0,\omega)]$ dielectric tensor of the medium. Assuming $\overleftrightarrow{\epsilon}(\omega)$ to be diagonal, the resulting polarizability is [17]

$$\alpha(\omega,k_x,k_y) = \frac{\sqrt{\epsilon_{zz}(k_x^2\epsilon_{xx}+k_y^2\epsilon_{yy})/K^2}-1}{\sqrt{\epsilon_{zz}(k_x^2\epsilon_{xx}+k_y^2\epsilon_{yy})/K^2}+1} \tag{2}$$

where $K = \sqrt{k_x^2+k_y^2}$ is the norm of the wave vector parallel to the surface [Fig. 1(c)], and the dependence on ω arises from the diagonal components of $\overleftrightarrow{\epsilon}(\omega)$: $\epsilon_{xx}(\omega)$, $\epsilon_{yy}(\omega)$, and $\epsilon_{zz}(\omega)$. Note that in the case of an isotropic crystal, the well-known expression $(\epsilon-1)/(\epsilon+1)$ is retrieved. The energy loss probability per unit angular frequency and per unit electron path length finally reads

$$\frac{d^2P(\omega,\mathsf{b})}{d\omega dx} = \frac{e^2}{(2\pi)^2 v^2\epsilon_0\hbar} \times \int_{-\infty}^{\infty} \mathrm{Im}\left[\alpha\left(\omega,\frac{\omega}{v},k_y\right)\right]\frac{e^{-2\mathsf{b}\sqrt{k_y^2+(\frac{\omega}{v})^2}}}{\sqrt{k_y^2+(\frac{\omega}{v})^2}}dk_y \tag{3}$$

where $k_x = \omega/v$ is the momentum transfer along the electron trajectory. In this expression, the imaginary part of the polarizability of the specimen $\mathrm{Im}[\alpha]$ multiplies a kinematic factor (depending on the electron trajectory and velocity) acting as a low-k, low-ω filter [18].

The microscopic behavior of the specimen is therefore entirely described by the low-frequency dielectric tensor $\overleftrightarrow{\epsilon}(\omega)$, which can be evaluated from first-principles calculations using the expression [19,20]

$$\epsilon_{\alpha\beta}(\omega) = \epsilon_{\alpha\beta}^{\infty} + \frac{4\pi}{\Omega}\sum_m \frac{Z_{m,\alpha}^* Z_{m,\beta}^*}{\omega_m^2-(\omega+i\Gamma_m)^2} \tag{4}$$

where α and β are Cartesian-coordinates indices, m runs over the phonon modes, Ω is the crystal unit-cell volume, ω_m are the frequencies of the phonons calculated at zero macroscopic electric field (TO modes), $\epsilon_{\alpha\beta}^{\infty}$ is the electronic dielectric tensor [i.e., the value of $\epsilon_{\alpha\beta}(\omega)$ for frequencies much higher than the typical long-wavelength TO phonon frequencies], and $Z_{m,\alpha}^*$ are the Born effective charge tensors (the coefficient of proportionality between the macroscopic polarization per unit-cell created in direction α and a cooperative displacement of the atoms following the phonon mode m). Finally, Γ_m is a broadening parameter accounting for the finite lifetime of the vibration. The numerators in Eq. (4) are usually called the mode oscillator strengths. The quantities ω_m, ϵ^{∞}, and Z^* can be calculated for a generic system entirely from first-principles [20].

The structure and vibrational properties (ω_m, ϵ^{∞}, and Z^*) of β-guanine were determined within DFT by using the QUANTUM ESPRESSO [21] package. Calculations were

TABLE I. Comparison between the experimental (taken from Ref. [13], space group $P112_1/b$) and optimized lattice parameters of β-guanine using both the GGA-PBE exchange-correlation only (PBE) and adding dispersion corrections (PBE + D2). Relative differences with respect to measurements are in parentheses.

	Experiment	PBE	PBE + D2
a (Å)	3.629	4.321 (+20%)	3.496 (−3.5%)
b (Å)	9.813	9.836 (+0.2%)	9.684 (−1.3%)
c (Å)	18.427	18.646 (+1.2%)	18.447 (+0.1%)
γ (°)	118.04	115.77	118.33

performed using ultrasoft pseudopotentials [22] with plane-wave and charge-density cutoffs of 60 and 600 Ry, respectively. The Brillouin zone was sampled using a $6 \times 2 \times 1$ **k**-point Monkhorst-Pack grid [23] and the generalized gradient approximation of Perdew, Burke, and Ernzerhof [24] (GGA-PBE) employed for exchange and correlation together with Grimme's dispersion corrections [25]. Atomic structure and crystal cell parameters were fully relaxed by energy minimization (Table I). The use of dispersion corrections clearly improves the treatment of interlayer interactions, for which bare GGA hardly predicts any binding [13]. Vibrational properties have therefore been calculated within this approximation [26].

β-guanine is a biaxial crystal of symmetry lower than orthorhombic. As a consequence, the axes diagonalizing the real and imaginary parts of its dielectric tensor are frequency dependent and, in general, do not coincide [27]. In our case, the monoclinic symmetry only fixes one principle axis along the twofold screw axis of the $P112_1/b$ crystal, i.e., along c. Choosing a second axis perpendicular to the molecular plane (Fig. 2), brings numerically both parts of the dielectric tensor close to a diagonal form. As this approximation is excellent in the 100–500 meV energy range of interest for these experiments, we will consider these axes as frequency independent.

The dielectric tensor calculated from Eq. (4) is shown in Fig. 2. A large number of modes contribute to the dielectric tensor leading to a strong frequency dependence, enhanced by the use of a constant, phenomenological damping parameter $\Gamma_m = 4$ cm^{-1}. Note that Γ_m is the only parameter in Eq. (4) which is not evaluated from first principles but set to an arbitrary value, here much smaller than the energy resolution currently accessible in EELS. Symmetry arguments help rationalize the large number of resonances observed numerically in Fig. 2. β-guanine crystallizes in the $P112_1/b$ space group with 16 atoms (forming the molecule) in the $4e$ Wyckoff position. A factor group analysis therefore gives the following decomposition:

$$\Gamma_{\text{vib}} = 48A_g \oplus 48A_u \oplus 48B_g \oplus 48B_u.$$

Subtracting the acoustic modes $A_u \oplus 2B_u$, we are left with 189 modes, among which 93 are odd under inversion symmetry. These modes only, decomposing as $47A_u \oplus 46B_u$, can generate a macroscopic polarization and therefore bring a nonzero contribution to the dielectric tensor.

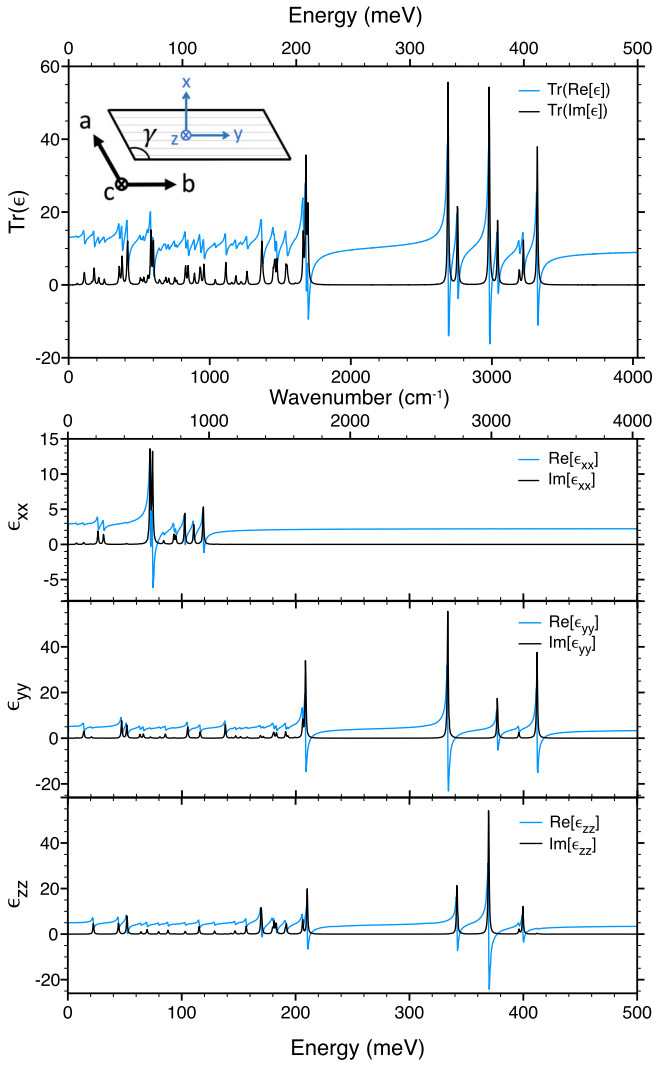

FIG. 2. Local dielectric tensor $\overleftrightarrow{\epsilon}(\omega)$ of β-guanine in the infrared domain of frequencies calculated according to Eq. (4) with a damping parameter $\Gamma_m = 4$ cm^{-1}. The trace of the tensor is shown in the upper panel and the three diagonal components in the lower panel.

A close inspection of Fig. 2 reveals that all modes above 1000 cm^{-1} (∼120 meV), i.e., modes essentially accessible in EELS, correspond to in-plane atomic displacements. Two groups are then clearly separated in this energy range: (i) between 2500 and 3500 cm^{-1} (∼310–435 meV), modes are exclusively associated with N-H, C-H, or NH_2 stretching whereas (ii) between 1000 and 2000 cm^{-1} (∼120–250 meV), they involve in-plane bending of these bonds hybridized with stretching of bonds arising within the pyrimidine and imidazole rings.

The theoretical vibrational EELS spectrum calculated from Eq. (3) and based on this dielectric tensor is shown in Fig. 3. This spectrum corresponds to the geometry depicted

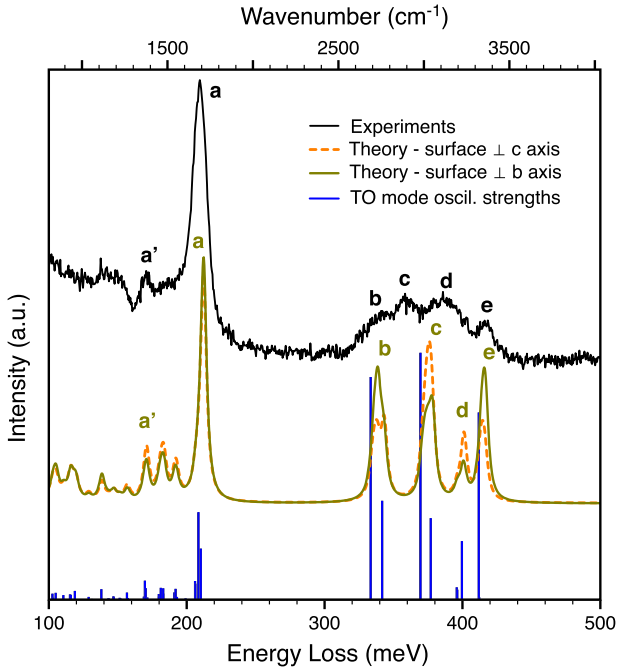

FIG. 3. Comparison between the experimental (Ref. [2]) and theoretical vibrational EELS spectra of β-guanine. Two spectra have been calculated, corresponding respectively to a surface perpendicular to the crystal c axis, as depicted in Fig. 1(c), and perpendicular to the crystal b axis. The 60 keV electron beam is perpendicular to the molecular plane and travels at a distance of $\mathsf{b} = 30$ nm from the specimen edge. Blue sticks show the theoretical TO mode oscillator strengths and frequencies.

in Fig. 1(c), for a surface perpendicular to the crystal c axis. The spectrum corresponding to an additional geometry, i.e., for a surface perpendicular to the crystal b axis, is also shown. These spectra have been calculated for 60 keV electrons and an impact parameter $\mathsf{b} = 30$ nm. Finally, to account for the energy resolution of the experiments, a Lorentzian broadening of full-width at half maximum of 5 meV has been applied. It appears that the peaks in the theoretical EELS spectra are systematically blue-shifted with respect to the TO modes. This effect results from the nonpenetrating geometry of the experiment, where the relevant physical quantity is the imaginary part of the polarizability $\alpha(\omega)$, whose poles have energies between the bulk TO and LO modes. The good overall agreement between experimental and calculated spectra allows for a clear identification of all the modes associated with the experimental peaks, labeled from a' to e in the figure (Table II).

Modes arising at high energy are well separated and correspond to weakly hybridized bond vibrations. Starting with the highest energies, peak e can be attributed purely to antisymmetric stretching of the NH_2 group. Peak d arises from both symmetric stretching of the NH_2 group and C8-H stretching, as these modes occur in the same energy range. The latter only brings a very weak contribution to the theoretical peak intensity. This is related to the predominantly covalent character of the C-H bond resulting in small Born effective charges on the H atom. This result correlates well with the fact that, unlike the polar N-H and NH_2 groups, the C8-H group is not involved in hydrogen bonding, as seen in Fig. 1(a).

Peaks b and c correspond, respectively, to N1-H and N7-H bond stretchings. Remarkably, our analysis shows that the frequency shift of these stretching modes, primarily induced by the different intermolecular hydrogen bonds in which they are involved—N1-H$\cdots$N and N7-H$\cdots$O, see Fig. 1(a)—can be detected experimentally in EELS. This analysis differs from a previous interpretation of these spectral features [2]. Finally, the overestimation of the peak intensities in the 2500–3500 cm^{-1} range of the theoretical spectrum might be partially attributed to the presence of anharmonic broadening induced by hydrogen bonds [28].

At lower energies, peaks a' and a are associated with groups of modes involving highly hybridized bond vibrations and, in particular, stretching of bonds within the pyrimidine and imidazole rings. Although the most intense peak a involves NH_2 scissoring and N1-H bending, the spectral intensity results essentially from bond stretching involving C6 and O atoms, which hold the largest effective charges in the molecule [Fig. 4(a)]. Along the same line, peak a' also visible and fairly intense in IR spectroscopy [2,29], arises from a group of modes involving NH_2 rocking, N1-H and C8-H bending together with a large number of intraring bond stretching modes [Fig. 4(b)]. It is not possible to assign

TABLE II. Dominant components of the modes associated with the major structures visible in the vibrational electron energy loss spectrum of β-guanine. The range of theoretical TO mode frequencies contributing to the different peaks is given. The following convention is employed to describe the type of vibration of a single bond: ν stretching; δ: in-plane bending; and of groups with two identical bonds ν_s: symmetric stretching; ν_a: antisymmetric stretching; δ_s: scissoring; δ_a: rocking.

Experiments [2]		Theory	
Peak	ω (cm^{-1})	ω_{TO} (cm^{-1})	Dominant contributions
e	3277	3322–3324	$\nu_a(NH_2)$
d	3078	3193–3223	$\nu_s(NH_2)$; ν(C8-H)
c	2846	2981–3041	ν(N7-H)
b	2663	2689–2756	ν(N1-H)
a	1666	1662–1695	$\delta_s(NH_2)$; ν(C6 = O); ν(C2-N10); δ(N1-H); ν(C2-N3); ν(C2-N1); ν(C5-C6)
a'	1379	1362–1373	$\delta_a(NH_2)$); δ(N1-H); δ(C8-H); δ(N7-H); ν(C4-C5); ν(C5-N7); ν(C4-N9); ν(C2-N1); ν(C4-N3)

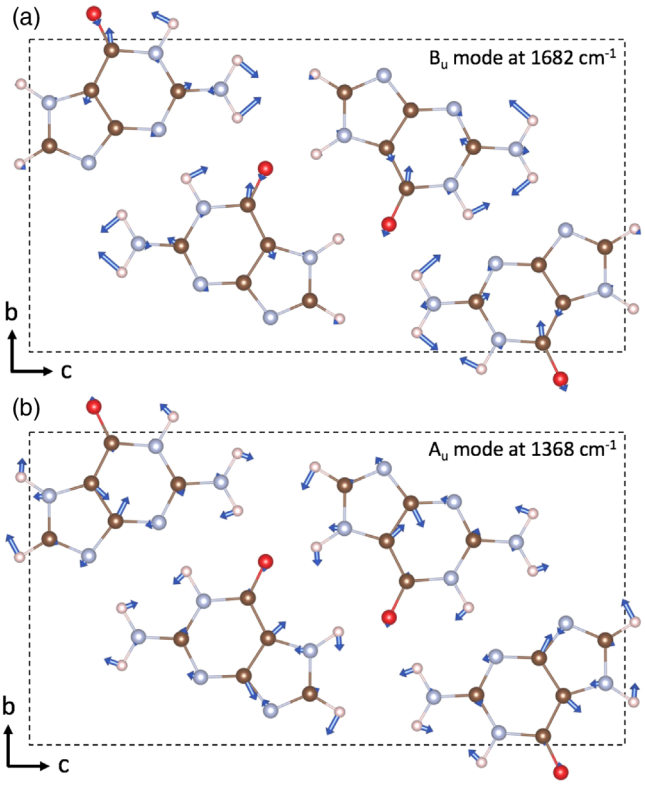

FIG. 4. Schematic representation of two modes contributing respectively to (a) peak *a* found experimentally at 1666 cm^{-1} and (b) peak *a*′ at 1379 cm^{-1} in the EELS spectrum shown in Fig. 3.

a particular bond vibration to this peak which results from collective movements of atoms holding similar effective charges. The absence of the predicted additional two peaks of similar intensities between 1400 and 1600 cm^{-1} in the experimental spectrum might be due to the limited energy resolution and signal-to-noise ratio available in EELS as they are visible in IR spectroscopy [2,29].

Concluding, the present work provides solid ground to improve the modeling and the interpretation of vibrational EELS acquired under experimental conditions where long-range dipole scattering dominates. In particular, first-principles calculations based on the DFT framework lead to unambiguous assignment of the peaks visible on the experimental spectrum of β-guanine. We remark that the interpretation of vibrational EELS data is still based on empirical models or on a direct comparison with known references. In the presence of large systems, this kind of approach might be incomplete and even misleading making the use of first-principles approaches highly desirable.

This work was granted access to the HPC resources of IDRIS under the allocation 2016-i2016097218 made by GENCI (Grand Equipement National de Calcul Intensif). G. R. is very thankful to P. Rez and K. March for providing the original EELS experimental data shown in Fig. 3.

*guillaume.radtke@impmc.upmc.fr

[1] O. L. Krivanek, T. C. Lovejoy, N. Dellby, T. Aoki, R. W. Carpenter, P. Rez, E. Soignard, J. Zhu, P. E. Batson, M. J. Lagos, R. F. Egerton, and P. A. Crozier, Nature (London) **514**, 209 (2014).
[2] P. Rez, T. Aoki, K. March, D. Gur, O. L. Krivanek, N. Dellby, T. C. Lovejoy, S. G. Wolf, and H. Cohen, Nat. Commun. **7**, 10945 (2016).
[3] M. J. Lagos, A. Trügler, U. Hohenester, and P. E. Batson, Nature (London) **543**, 529 (2017).
[4] H. Ibach and D. L. Mills, *Electron Energy Loss Spectroscopy and Surface Vibrations* (Academic Press, London, 1982).
[5] C. Dwyer, Phys. Rev. B **89**, 054103 (2014).
[6] N. R. Lugg, B. D. Forbes, S. D. Findlay, and L. J. Allen, Phys. Rev. B **91**, 144108 (2015).
[7] C. Dwyer, T. Aoki, P. Rez, S. L. Y. Chang, T. C. Lovejoy, and O. L. Krivanek, Phys. Rev. Lett. **117**, 256101 (2016).
[8] R. F. Egerton, Microsc. Microanal. **20**, 658 (2014).
[9] R. F. Egerton, Ultramicroscopy **159**, 95 (2015).
[10] P. Crozier, T. Aoki, and Q. Liu, Ultramicroscopy **169**, 30 (2016).
[11] A. Levy-Lior, E. Shimoni, O. Schwartz, E. Gavish-Regev, D. Oron, G. Oxford, S. Weiner, and L. Addadi, Adv. Funct. Mater. **20**, 320 (2010).
[12] D. Gur, B. Leshem, M. Pierantoni, V. Farstey, D. Oron, S. Weiner, and L. Addadi, J. Am. Chem. Soc. **137**, 8408 (2015).
[13] A. Hirsch, D. Gur, I. Polishchuk, D. Levy, B. Pokroy, A. J. Cruz-Cabeza, L. Addadi, L. Kronik, and L. Leiserowitz, Chem. Mater. **27**, 8289 (2015).
[14] P. Batson, Ultramicroscopy **11**, 299 (1983).
[15] A. Howie, Ultramicroscopy **11**, 141 (1983).
[16] D. Taverna, M. Kociak, V. Charbois, and L. Henrard, Phys. Rev. B **66**, 235419 (2002).
[17] Ph. Lambin, P. Senet, A. Castiaux, and L. Philippe, J. Phys. I **3**, 1417 (1993).
[18] M. Kociak, Ph.D. Thesis, Université Paris Sud—Paris XI, 2001.
[19] X. Gonze and C. Lee, Phys. Rev. B **55**, 10355 (1997).
[20] S. Baroni, S. de Gironcoli, A. Dal Corso, and P. Giannozzi, Rev. Mod. Phys. **73**, 515 (2001).
[21] P. Giannozzi *et al.*, J. Phys. Condens. Matter **21**, 395502 (2009).
[22] K. F. Garrity, J. W. Bennett, K. M. Rabe, and D. Vanderbilt, Comput. Mater. Sci. **81**, 446 (2014).
[23] H. J. Monkhorst and J. D. Pack, Phys. Rev. B **13**, 5188 (1976).
[24] J. P. Perdew, K. Burke, and M. Ernzerhof, Phys. Rev. Lett. **77**, 3865 (1996).
[25] S. Grimme, J. Comput. Chem. **27**, 1787 (2006).
[26] Note that Eq. (4) is calculated from the bulk phonon properties. This is justified by the fact that the impact parameter b, which acts in Eq. (3) as a momentum cutoff, is of the order of a few tens of nm.
[27] L. D. Landau and E. M. Lifshitz, *Electrodynamics of Continuous Media* (Pergamon Press, New York, 1960).
[28] M. Bonn, M. J. P. Brugmans, A. W. Kleyn, R. A. van Santen, and H. J. Bakker, Phys. Rev. Lett. **76**, 2440 (1996).
[29] R. P. Lopez, M. P. M. Marques, R. Valero, J. Tomkinson, and L. A. E. Batista de Carvalho, Spectroscopy (Amsterdam) **27**, 273 (2012).